Progress in Photovoltaics: Research and Applications

WILEY

PROGRESS IN PHOTOVOLTAICS

RESEARCH ARTICLE OPEN ACCESS

Tips and Tricks for a Good Encapsulation for Perovskite-Based Solar Cells

Quiterie Emery[1] | Lea Dagault[2] | Mark Khenkin[1] | Nikoleta Kyranaki[2] | Wander Max Bernardes de Araújo[1] | Ulas Erdil[1,3] | Matthias Demuylder[2] | Stephane Cros[2] | Rutger Schlatmann[1] | Bernd Stannowski[1] | Carolin Ulbrich[1]

[1]Helmholtz-Zentrum Berlin für Materialen und Energie, Berlin, Germany | [2]Département Des Technologies Solaires, Université Grenoble Alpes, Commissariat à l'énergie atomique et aux énergies alternatives (CEA), Le Bourget-du-Lac, France | [3]Faculty of Chemistry, Bielefeld University, Bielefeld, Germany

Correspondence: Mark Khenkin (mark.khenkin@helmholtz-berlin.de) | Stephane Cros (stephane.cros@cea.fr)

Received: 10 June 2024 | **Revised:** 15 November 2024 | **Accepted:** 2 January 2025

Funding: This work was supported by the European Climate, Infrastructure and Environment Executive Agency and European Union's Horizon Europe (101006715, 101084251).

Keywords: damp heat | encapsulation | perovskite solar cell | perovskite test | stability | thermal cycling | vacuum lamination

ABSTRACT

Encapsulation is a critical topic to ensure the successful implementation of perovskite photovoltaics. Recently, vacuum lamination has been shown as a promising approach that combines compatibility with current industrial processes in conventional photovoltaic (PV) manufacturing and suitability to achieve good results with perovskites. Here, we explore some of the attractive encapsulation materials in terms of their ability to prevent moisture ingress, withstand elevated temperatures, and have suitable mechanical properties to avoid thermomechanical issues. We utilized the previously suggested concept of the "perovskite test," an optical test with simple sample fabrication, for evaluating encapsulation quality and validated the findings with the full solar cell stack. Unsurprisingly, encapsulants without an edge sealant showed insufficient protection from moisture. Ionomer in combination with butyl edge seal showed the best barrier properties; however, this stack led to rapid delamination of the cell layers in thermal cycling tests. Configuration with only edge sealant does not have such an issue in principle (no mechanical stress applied), but an absence of the polymer in the stack is unfavorable in terms of optical design and sometimes showed perovskite degradation that we assign to trapped moisture in the butyl itself. Polyolefin with butyl edge sealant is not free of degradation but showed the most promising compromise by passing the damp heat test and showing fewer issues in the thermal cycling experiments. In general, our material study and optimization presented in this manuscript show that a holistic approach is needed when choosing an optimal encapsulation scheme for perovskite devices.

1 | Introduction

In the realm of renewable energy, perovskite solar cells (PSCs) have emerged as promising contenders, offering a cost-effective and highly efficient alternative to traditional silicon-based photovoltaic technologies [1]. However, the commercial viability of PSCs has been hindered by their sensitivity to environmental factors, notably moisture and oxygen, posing potential threats to both stability and overall performance [2]. To address these challenges and unlock the full potential of PSCs, researchers and engineers are increasingly turning to encapsulation technologies [3–10].

Quiterie Emery and Lea Dagault contributed equally to this work.

Encapsulation serves as a protective barrier, safeguarding the sensitive perovskite materials from external influences and thereby extending the lifespan of solar cells. A successful encapsulation for PSCs necessitates a careful consideration of key properties. First and foremost, impermeability to moisture and oxygen is paramount to shield the perovskite layer from degradation. The encapsulating material should exhibit excellent chemical stability to withstand the harsh conditions encountered during the solar cell's life cycle. The encapsulation procedure should be mild enough to not damage the PSC, which particularly limits the maximum processing temperature. It is important to distinguish between degradation and damage in PSCs. Here, "degradation" refers to the long-term effects experienced by PSCs under typical operating conditions, such as material breakdown over time due to environmental stressors. In contrast, "damage" describes the immediate impact of processing conditions, including factors like temperature and pressure, which can cause harm if not carefully controlled. This distinction is important as processing conditions may exceed operational limits, potentially leading to short-term damage rather than long-term degradation. Additionally, transparency is crucial to allow for optimal light absorption, ensuring that the encapsulation does not compromise the energy conversion efficiency [11]. Furthermore, flexibility and compatibility with the perovskite layer are essential to accommodate any structural changes or stresses [12].

Glass/glass encapsulation stands out as a promising pathway for the commercialization of PSCs. Indeed, glass is renowned for its impermeability, chemical stability, and optical transparency [13]. Glass/glass encapsulation not only shields the cells from moisture and oxygen but also provides a robust physical barrier against mechanical stresses. Various encapsulants can be associated to glass to provide an adequate encapsulation. Ethylene vinyl acetate (EVA) has a well-established track record in the solar industry and offers excellent transparency and adhesion properties. However, it is prone to discoloring and delamination, and its acetic acid byproduct can degrade the perovskite. The most common alternatives reported in the literature appear to be ionomers and polyolefin elastomers (POEs) [14–17]. Nevertheless, POEs are cross-linking polymers that require a high processing temperature that is not always compatible with the thermal sensitivity of perovskite devices. Ionomer, on the other hand, can be processed at lower temperatures since they are thermoplastics that form physical cross-links via ionic bonds [18]. Nonetheless, they suffer from other issues such as inferior adhesion to glass and PV cell interfaces compared to traditional materials like EVA [19]. In order to reduce moisture ingress, a desiccant-filled polyisobutylene (PIB or butyl) is often added to the edges [20]. In addition to providing a very low water vapor transmission rate (WVTR) (1×10^{-2} to 1×10^{-3} g/(m^2 day) and a low glass transition temperature [21], PIB can be processed at a lower temperature than ionomers or POEs. Therefore, it has sometimes been reported to be used alone and questions the necessity to combine it with a transparent polymer for a moisture-proof encapsulation of PSCs. However, some groups have shown that a polymer encapsulant improves stability and reliability of PSCs, particularly by preventing the escape of volatile products of perovskite decomposition reaction [22–24].

In this work, we study the important characteristics to consider when choosing an appropriate encapsulation for PSCs. From physical and mechanical properties of the polymer encapsulants to damp heat and thermal cycling test on full devices, we show how to assess the quality of an encapsulation to maximize the lifespan of PSCs. Beyond technical considerations, this exploration aims to empower the scientific community with practical insights, ensuring that encapsulation becomes not just a protective measure but a pivotal driver for advancing the commercial viability and widespread adoption of perovskite-based technology.

2 | Methods

In order to find the most suitable encapsulation for PSCs, ionomer (Mitsui PV8729D) and polyolefin (Mitsui TR02BA-50T) encapsulants processed at different temperatures (130°C or 150°C) are compared. Their use alone or in combination with a butyl edge sealant (Quanex SET LP03) is evaluated and compared with the use of edge sealant alone, processed either with a vacuum laminator (Meier Solar Solution, ICOLAM 10/08) or with a heat press (RICOO, T505). Samples encapsulated with an encapsulant (ionomer or polyolefin) alone or with an encapsulant and an edge sealant are laminated in the vacuum laminator in three steps: pull vacuum for 4 min then ramp press to 900 mbar for 2 min and press with 900-mbar pressure for 14 min. Samples encapsulated with edge sealant alone in the vacuum laminator are laminated with the same three steps but with only 500-mbar pressure applied for 8 min. For samples encapsulated with the heat press, the pressure applied cannot be estimated by the setup, but the samples are pressed for 100 s at 120°C.

Figure 1a shows the test samples stack that contains glass/ITO/400 nm of $Cs_{0.17}FA_{0.83}PbI_{2.49}Br_{0.51}$ perovskite/100 nm of ITO, as well as an encapsulant layer and/or edge sealant and a rigid glass cover. For encapsulations without and with edge sealant, the perovskite initial areas are respectively 4×4 and 2×2 cm^2. These samples are exposed to damaging conditions, generally damp heat (85°C, 85% relative humidity), to evaluate water ingress within the stack. The lateral permeation of the encapsulated stacks is evaluated on these passive samples with an optical test, referred to as the "perovskite test" or PK-test [25]. A camera setup and image treatment software [26] are used to determine the remaining "active area" and the "equivalent

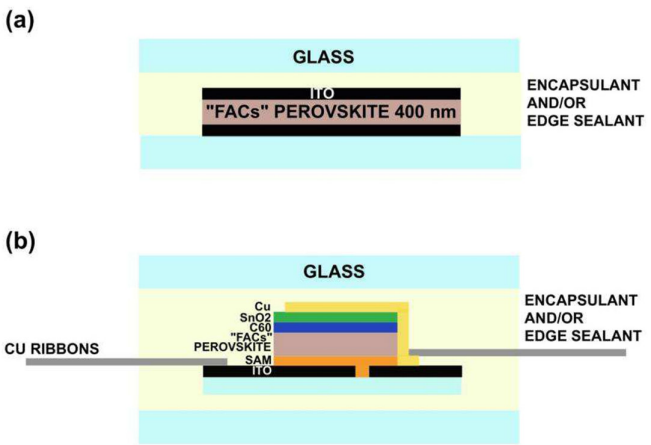

FIGURE 1 | (a) "Perovskite test" stack and (b) encapsulated perovskite solar cell stack.

thickness" by identifying color changes. The active area corresponds to the surface area where the perovskite thickness remains above 180 nm, and the "equivalent thickness" is the average perovskite thickness remaining in the active area.

Figure 1b presents PSCs with a p–i–n structure and a layer configuration of ITO|2PACz|$Cs_{0.17}FA_{0.83}PbI_{2.49}Br_{0.51}$|$C_{60}$|$SnO_2$|Cu, which were fabricated, encapsulated, and measured according to the same procedure as described previously [17].

Table 1 provides a summary of the aging conditions and associated figures for the sample types depicted in Figure 1.

Additional material characterization is performed on the encapsulation materials to infer their thermal and mechanical properties, as well as their permeation. A dynamical mechanical analysis (DMA) Q800 tool from TA Waters is used to perform temperature sweeps up to 100°C and evaluate the rigidity and glass transition temperature. DSC measurements were performed from −20°C to +200°C with a Q20 from TA Waters, following a method similar to [27] to evaluate the cross-linking temperature of the POE. The transversal permeation measurements were done with water vapor with an internal tool or with helium using the QHV4 tool from Vinci Technologies [28, 29]. The permeation experiments are performed at 38°C on circular samples with a 6-cm diameter.

3 | Encapsulant Barrier Effectivity and How Its Properties Impact the Degradation

In order to investigate the barrier properties of the encapsulants, water vapor and helium transmission experiments were performed on samples of polyolefin and ionomer laminated at different temperatures. The ionomer is not supposed to cross-link during lamination, while the POE contains some cross-linking agents and should react near 140°C. The transverse permeability values obtained are shown in Figure 2, for POE laminated at 100°C, 130°C, and 150°C. These results are compared with ionomer laminated at 140°C. All POE samples present a water permeability above 0.01 g mm/m²/d/mbar, and helium permeability above 1×10^{-4} g mm/m²/d/mbar. The differences in permeability values of the POE processed at various temperatures are relatively small, with overlapping standard deviations, suggesting that they may not be statistically significant. However, the permeability of the POE seems to increase with lamination temperature, which implies that higher lamination temperatures could adversely affect the barrier properties of this material (see Figure S1 for more

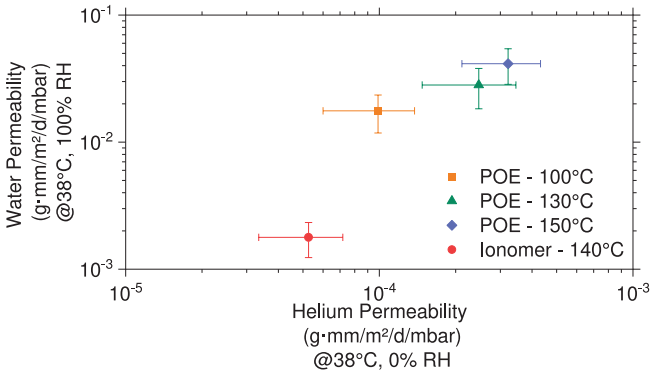

FIGURE 2 | Water permeability versus helium permeability for POE samples laminated at 100°C, 130°C, or 150°C, compared to ionomer laminated at 140°C. More details on helium permeability are shown in Figure S1.

TABLE 1 | Summary table of the aged samples and their associated figures.

Sample stack	Encapsulation	Aging conditions	Associated figure
Perovskite test stack	POE, 130°C	Damp heat (85°C/85% RH)	Figure 3
	POE, 150°C		
	Ionomer, 130°C		
	Butyl only, vacuum laminator, 120°C		Figure 6
	Butyl only, heat press, 120°C		
	Butyl only, vacuum laminator, 120°C		Figure S5
	Butyl only, vacuum laminator, 150°C		
	Butyl + POE, 150°C		Figure 4
	Butyl + ionomer, 150°C		
	No encapsulation	Room temperature, glovebox	Figure S6
		85°C, glovebox	
Full solar cell stack	Butyl + POE, 150°C	Damp heat (85°C/85% RH)	Figure 5
		85°C, ambient atmosphere	
	Butyl only, 120°C	Room temperature, ambient atmosphere	Figures 7 and S8
	Butyl + POE, 150°C	Thermal cycling	
	Butyl + ionomer, 150°C		

details). This trend is expected, as an increased degree of cross-linking in a polymer typically reduces its crystallinity, resulting in a higher WVTR [30]. The ionomer shows a much lower water permeability, below 2×10^{-3} g mm/m^2/d/mbar, highlighting better resistance to water ingress.

The lateral permeation of the laminated stacks was studied on passive structures, using the PK-test method. A first series of samples was manufactured by laminating POE at 130°C and 150°C, as well as ionomer at 130°C on the PK-test stack. Two samples were tested for each condition and placed in damp heat (85°C, 85% RH) for up to 1000 h. Figure 3 presents the evolution of equivalent thickness (a) and active area (b) as a function of time: It can be observed that both metrics drop quickly for POE, in less than 100 h. The measurements for the samples of different lamination temperatures overlay. This indicates a rapid water ingress into the stack, which causes the decomposition of the perovskite layer. Samples with ionomer show a different behavior: The active area remains stable for 500 h of damp heat treatment while the equivalent thickness decreases only slightly. More information can be inferred from the images themselves, using thickness maps (Figure S2) or the raw images (Figure S3). The thickness maps of POE samples after a very short aging period (24 h) exhibit a gradient from the center to the corners. This suggests that water enters from the sides, which is confirmed by the raw images in Figure S3, where nonuniform changes appear in the polymer for both lamination temperatures. These variations lead to incomplete surface coverage, facilitating water ingress. Notably, lamination at 150°C showed only isolated bubble formation, whereas more pronounced changes, including a fingerlike pattern, were evident at 130°C (see Figure S3). This observation is consistent with Figure S2, which shows that after 24 h of damp heat aging, the perovskite layer's thickness is greater for samples laminated at 150°C than at 130°C. This suggests that a lamination temperature of 130°C may be insufficient or that the lamination duration was too short, potentially preventing the polymer melt from achieving proper surface wetting due to high melt viscosity. In contrast, this fingerlike pattern was not observed in the ionomer samples. The perovskite thickness decreases more gradually and uniformly across the whole surface, as shown in Figure S2c and in the stable active area observed over the first 500 h of aging. The uniform decrease in thickness may be attributed to water trapped within the encapsulant or, more likely, to rapid water permeation at the interfaces with glass, as discussed in [25]. Indeed, it has been shown that ionomer may exhibit poor adhesion to glass if the lamination process is suboptimal [31]. However, this hypothesis was not investigated further.

A second series of passive samples was studied additionally using butyl as the edge sealant. Figure 4 presents the equivalent thickness (a) and active area (b) as a function of time for POE and ionomer laminated at 150°C. This time, both materials have an almost identical behavior over time: The active area is perfectly stable, while there is a slight equivalent thickness decrease. Overall, the samples resist water ingress much better with the applied edge sealant. The low permeation of butyl was confirmed with helium transmission tests, shown in Figure S1. As shown later, edge sealant is mandatory when it comes to protection from humidity, but the encapsulant is not. Barrier properties of the encapsulant might still however be relevant in some cases (such as moisture trapped in the butyl or glass crack in the field), and therefore, ionomer is a better choice than POE regarding water ingress. Additionally, we emphasize that humidity is only one stress factor; butyl edge seals do not act as barriers to oxygen. Moreover, other stressors, such as UV exposure and mechanical loads encountered in real operating conditions, are not addressed in DH tests and should be considered in future studies [32].

In order to translate the results of the PK-test to full cells, we encapsulated three devices with four cells each in a similar fashion to the samples encapsulated with butyl + POE and exposed them to damp heat (85°C, 85% RH) or to 85°C in ambient atmosphere in an oven for around 2000 h. Figure 5 displays the normalized PCE over exposure time. The devices maintained on average more than 90% of their initial performance after 1000 h and more than 85% of their initial performance after 2000 h in the damp heat chamber. The slow performance drop, mainly caused by FF and a Jsc drop, is shown to be due to thermal degradation rather than to an encapsulation failure as the samples from the same batch exposed to 85°C in ambient atmosphere also experience a similar decay. Nonetheless, it is possible that trapped moisture within the encapsulant could also be a contributing factor. Furthermore, after 1000 h, the samples lose around 8% of their performance, which correlates to the equivalent thickness

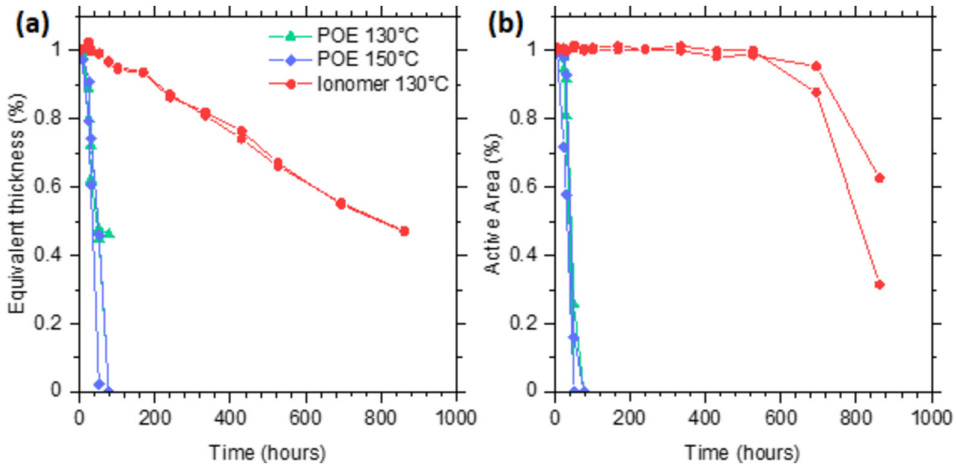

FIGURE 3 | Evolution of the (a) equivalent thickness and (b) active area of perovskite samples encapsulated with ionomer vs. POE and submitted to the PK-test.

drop, i.e., around 8%, determined in the PK-test. Note that this validates the PK-test as a representative method to probe the encapsulation quality; good moisture barrier properties confirmed by the PK-test guarantee good stability against moisture ingress in a full solar cell (all other stressors, of course, can trigger different degradation mechanisms and should be screened for in respective appropriate tests).

4 | The Importance of the Processing Conditions

Lamination at different temperatures was tested to evaluate how the lamination method impacts the properties of the POE encapsulant. We found in DSC measurements (Figure S4) that the cross-linking took place only for the 150°C lamination temperature. This finding may explain differences in the fingerlike patterning observed on passive samples exposed to damp heat conditions (Figure S3). We conclude that cross-linking induced by a higher lamination temperature may help prevent mechanical creep issues that could arise in operation [33]. However, as mentioned earlier, increased cross-linking typically raises the WVTR by reducing the crystallinity of polyethylene in the encapsulant films, which could pose a challenge if used without an edge sealant.

Butyl-only encapsulations ("only" means no encapsulant) were also tested, with different tools and temperatures. A first trial was made by encapsulating passive samples at 120°C either with a heat press or with a vacuum laminator. Figure 6 shows the extracted equivalent thickness and active area over time. Although visually similar, samples laminated with the heat press (green connected symbols in the figure) exhibit a rapid loss in both equivalent thickness and active area. The samples are fully degraded in less than 200 h, showing a fast ingress of water in the stack. This might be due to the nonoptimized encapsulation conditions, such as a lack of control of the applied pressure and insufficient pressure duration. Samples laminated with the vacuum laminator (black connected stars) show a stable active area, but a partial loss of equivalent thickness. This uniform thickness loss occurs until ~300 h and then slows down during the rest of the experiments. Given that the samples encapsulated with additional POE or ionomer did not exhibit this thickness decrease, we proposed three potential explanations. Our initial hypothesis posited that the aged butyl contained residual water, released during the damp heat exposure, which then reacted with the perovskite layer in the absence of an additional polymer barrier. A second hypothesis suggested that the encapsulation process at 120°C for butyl only, compared to 150°C for butyl + POE, might have insufficiently bonded the butyl to the glass, allowing moisture ingress. Our final hypothesis suggested thermal degradation during damp heat treatment in the absence of a polymer covering, as seen in *butyl-only* encapsulation.

To test these hypotheses, we conducted additional experiments. In one experiment, we examined the effect of butyl processing temperature on moisture ingress. Using fresh butyl rolls to eliminate moisture absorption, we found no significant difference in water ingress between lamination at 120°C and 150°C. As shown in Figure S5, passive samples encapsulated with butyl only at both temperatures remained stable after over 2500 h in damp heat conditions, refuting the second and third abovementioned hypotheses. This finding is consistent with the absence of

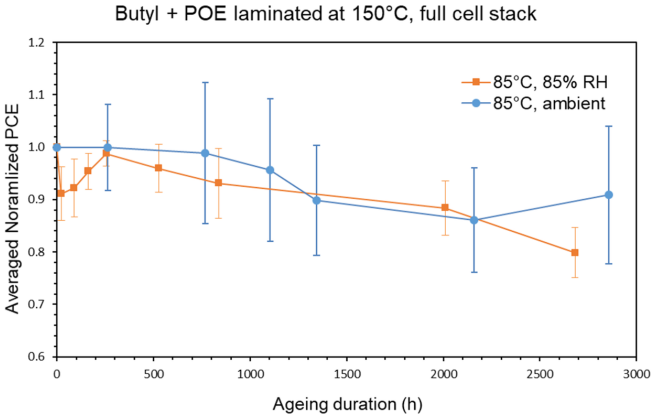

FIGURE 5 | Evolution of the normalized efficiency with standard deviation of perovskite solar cells encapsulated with butyl + POE during aging in the damp heat chamber at 85°C and 85% RH or in the oven at 85°C and ambient humidity. Average values are shown over respectively four and eight individual solar cells for samples exposed to damp heat and oven. Both curves represent general trends, and no outliers were observed.

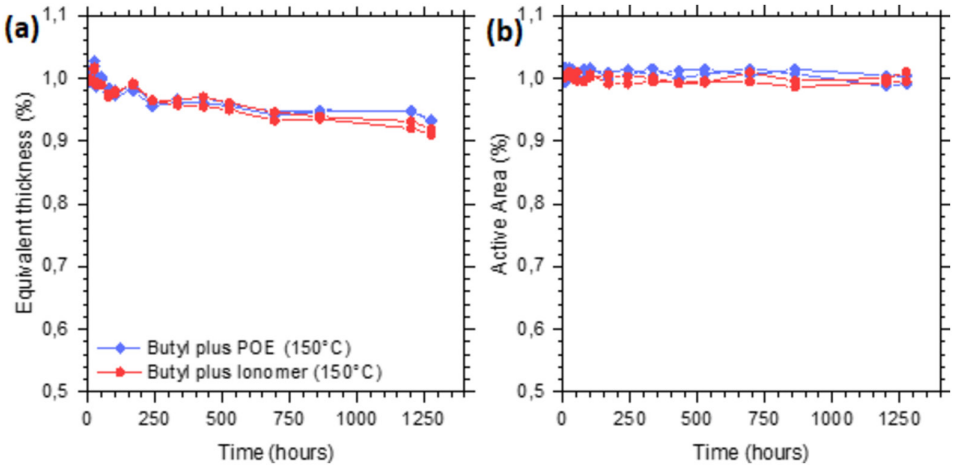

FIGURE 4 | Evolution of the (a) equivalent thickness and (b) active area of perovskite samples encapsulated with butyl edge sealant + ionomer vs. POE and submitted to damp heat conditions.

cross-linking in butyl, allowing flexibility in selecting an appropriate lamination temperature.

In another experiment, we conducted equivalent thickness and active area measurements, akin to the PK-test, on nonencapsulated samples aged in a glovebox. Half were exposed to 85°C on a hot plate while the others remained at room temperature. Samples subjected to 85°C displayed a noticeable loss of equivalent thickness, contrasting with those at room temperature, which showed no change (Figure S6). The presence of residual solvents in the glovebox, combined with heat, likely contributed to the observed thickness loss, indicating that water trapped within the materials during initial encapsulation could have caused the initial decrease. This underscores the importance of drying the butyl before lamination or using a fresh roll that did not absorb any moisture yet.

Based on our results, we conclude that adding a cover encapsulant in addition to an edge sealant does not necessarily improve cell stability. While other studies have indicated that an air gap within the encapsulation can contribute to instability [22, 34], we believe this effect may be limited to specific solar cell configurations, such as those with MA-based perovskites. However, we recommend using a cover encapsulant along with the edge sealant when scaling up device production, as it may contribute to better structural robustness for the module [14, 35].

5 | The Effect of the Encapsulant on the Mechanical Integrity of the Device

The three encapsulations that gave the best results in the lateral permeation test (butyl + POE, butyl + ionomer, and butyl only) were implemented on full devices and submitted to thermal cycling (cycles between −40 and 85°C according to the IEC 61215 standard). Two substrates with six cells each were tested for each encapsulation type, and an additional device that was encapsulated with butyl only was aged on-shelf and used as a reference. Figure 7 shows the evolution of the performance of the cells during thermal cycling. Both devices encapsulated with butyl + ionomer (marked in light and dark green [overlaying] in the figure) have delaminated already after the first cycle. In this case, the whole area of the device was completely delaminated. This is assumed to be due to a too high elastic modulus of the encapsulant that does not enable the dissipation of strain introduced by the difference in thermal expansion coefficients of the materials [36].

Two devices encapsulated with butyl + POE (light and dark blue) showed very different behaviors. One of them (marked light blue) started to delaminate after the fifth cycle (Figure S7) while the other one (dark blue) did not delaminate after 200 cycles. Unlike the case with ionomer, the delamination caused by POE was localized to some areas of the substrate. The substrate with delamination quickly lost efficiency compared to the second substrate that did not show such effect. Nevertheless, even the device that did not delaminate lost an average of 19% of its initial efficiency after 200 cycles, indicating that the cells themselves degraded (similar to the case of butyl only). It is not clear why in some cases we observe the delamination effect and in others do not. Speculatively, it might be related to uncontrolled manufacturing defect and should be a subject of separate studies.

DMA measurements were performed to elucidate how the thermomechanical properties of ionomer and POE influence the delamination. Figure 8 presents (a) the tan(δ) for POE laminated at

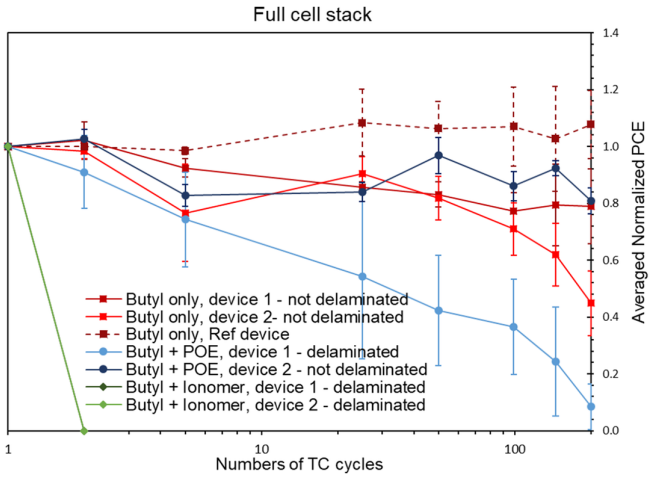

FIGURE 7 | Evolution of the PCE of samples encapsulated with butyl + ionomer vs. butyl + POE vs. butyl only during thermal cycling. Average values over three to six cells per device are shown with standard deviation. The curves for each device represent general trends, and no outliers were observed.

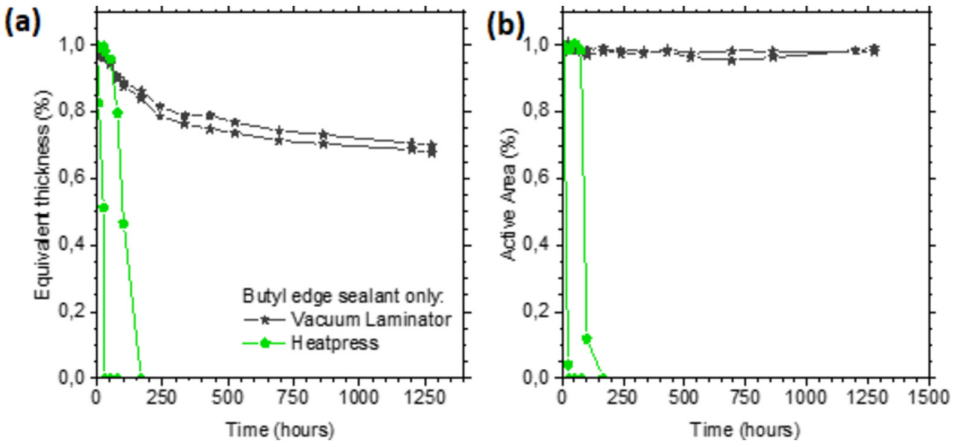

FIGURE 6 | Evolution of the (a) equivalent thickness and (b) active area of perovskite samples encapsulated with butyl edge sealant via a vacuum laminator vs. with a heat press and submitted to damp heat conditions.

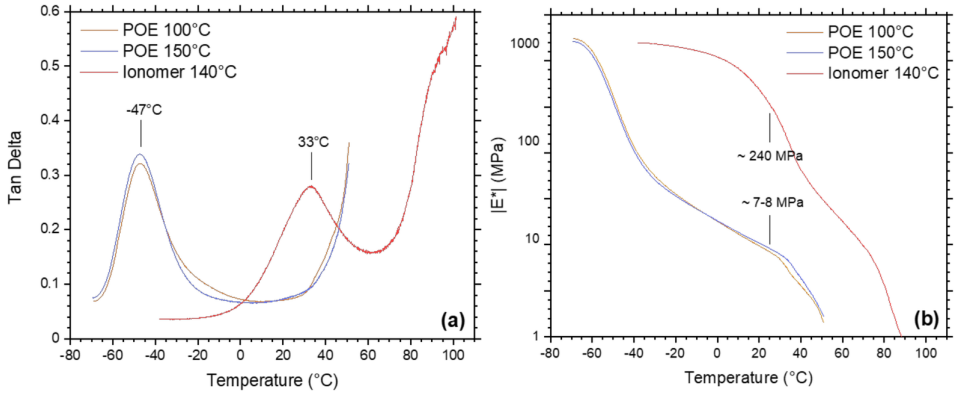

FIGURE 8 | DMA results on POE laminated at 100°C or 150°C, compared with ionomer laminated at 140°C. (a) Tan δ as a function of temperature, with peaks that correspond to the glass transition. (b) The stiffness evolution with temperature. The written values indicate the stiffness at room temperature.

100°C or 150°C and (b) the stiffness evolution with temperature for the same materials. The tan(δ) measurement allows us to study the evolution of the viscoelastic properties, and the peaks indicate the glass transition of the polymers [37]. It can be noticed that this temperature near −47°C for both POEs is outside of the thermal cycling range. For ionomer, this transition occurs near 33°C and, thus, occurs at every cycle. In addition, the complex modulus |E*| (used to estimate the stiffness evolution) in Figure 8b shows that the glass transition is accompanied by a drastic change in the rigidity of the material [38, 39]. Over the whole thermal cycle, the ionomer complex modulus covers a breadth of 1000 MPa. This likely causes strains within the stack, leading to delamination as soon as the first cycle. On the contrary, the POE complex modulus varies less within the cycle range and remains below 100 MPa: It seems that the material sometimes causes delamination but requires an accumulation of cycles. For further understanding, these results should be complemented with adhesion testing, as well as measurements of the thermal expansion coefficient.

Regarding the samples encapsulated with butyl only (marked in shades of red in Figure 7), none of them delaminated, since the butyl does not touch the cell's surface. However, the cells lost on average 38% of their initial performance after 200 cycles. Even without an encapsulant covering the cells, the latter tend to degrade when submitted to thermal cycling. Indeed, Jsc, Voc, and especially FF tend to drop with thermal cycles (Figure S8). This degradation is attributable to the aging conditions, as samples aged on-shelf did not demonstrate this decline in performance. Since such degradation is not related to the encapsulation, as fresh butyl was used, but probably to the PSC structure, the origin of such degradation goes beyond the scope of this study. Overall, this demonstrates that the challenge of choosing the right encapsulation is multifaceted and is not limited to simple good barrier properties against moisture and oxygen penetration.

6 | Conclusion

When selecting an appropriate encapsulant, several factors must be taken into account. We demonstrate via an optical test on passive samples that having an edge sealant is necessary and in principle sufficient for optimal barrier properties. However, an additional polymer encapsulant is also required, notably for optimized optics and to provide supplementary barrier properties, such as protection against moisture that could have been trapped in the edge sealant before processing. Comparing an ionomer and a polyolefin encapsulant, we find that the ionomer shows the most promising results in terms of barrier properties due to its superior permeability. Nevertheless, its high stiffness and glass transition temperature make it less favorable in terms of mechanical properties, resulting in cells quickly delaminating during thermal cycling. On the other hand, polyolefin combined with butyl emerges as the best compromise, offering sufficient moisture resistance while minimizing the risk of delamination. However, we recommend exploring softer encapsulant options to mitigate delamination entirely. It is worth noting that this study does not address other crucial aspects of encapsulants for PSCs, such as their lead containment capability and environmental impact, which should be the subject of a separate study. Above all, this study underscores the necessity of considering additional factors specific to PSCs, beyond those relevant to silicon solar cells.

Acknowledgments

These results have been achieved in the frame of the European Union's Horizon Europe financed project VIPERLAB (GA number 101006715). This project is cofunded by the European Union. Views and opinions expressed are however those of the author(s) only and do not necessarily reflect those of the European Union or the European Climate, Infrastructure and Environment Executive Agency (CINEA). Neither the European Union nor the granting authority can be held responsible for them. Open Access funding enabled and organized by Projekt DEAL.

Conflicts of Interest

The authors declare no conflicts of interest.

Data Availability Statement

The data that support the findings of this study are available from the corresponding author upon reasonable request.

References

1. H. S. Jung and N. G. Park, "Perovskite Solar Cells: From Materials to Devices," *Small* 11, no. 1 (2015): 10–25.

2. D. Wang, M. Wright, N. K. Elumalai, and A. Uddin, "Stability of Perovskite Solar Cells," *Solar Energy Materials and Solar Cells* 147 (2016): 255–275.

3. F. Matteocci, L. Cinà, E. Lamanna, et al., "Encapsulation for Long-Term Stability Enhancement of Perovskite Solar Cells," *Nano Energy* 30 (2016): 162–172.

4. Z. Liu, B. Sun, T. Shi, Z. Tang, and G. Liao, "Enhanced Photovoltaic Performance and Stability of Carbon Counter Electrode Based Perovskite Solar Cells Encapsulated by PDMS," *Journal of Materials Chemistry A* 4, no. 27 (2016): 10700–10709.

5. Y. Han, S. Meyer, Y. Dkhissi, et al., "Degradation Observations of Encapsulated Planar CH3NH3PbI3 Perovskite Solar Cells at High Temperatures and Humidity," *Journal of Materials Chemistry A* 3, no. 15 (2015): 8139–8147.

6. B. McKenna, J. R. Troughton, T. M. Watson, and R. C. Evans, "Enhancing the Stability of Organolead Halide Perovskite Films Through Polymer Encapsulation," *RSC Advances* 7, no. 52 (2017): 32942–32951.

7. S. Emami, J. Martins, R. Madureira, et al., "Development of Hermetic Glass Frit Encapsulation for Perovskite Solar Cells," *Journal of Physics D: Applied Physics* 52, no. 7 (2018): 074005.

8. E. Y. Choi, J. Kim, S. Lim, E. Han, A. W. Y. Ho-Baillie, and N. Park, "Enhancing Stability for Organic-Inorganic Perovskite Solar Cells by Atomic Layer Deposited Al2O3 Encapsulation," *Solar Energy Materials and Solar Cells* 188 (2018): 37–45.

9. J. Yin, J. Cui, H. Zhou, et al., "Encapsulation of UV Glue, Hydrophobicity of Binder and Carbon Electrode Enhance the Stability of Organic–Inorganic Hybrid Perovskite Solar Cells up to 5 Years," *Energy Technology* 8 (2020): 1–5.

10. Z. Fu, M. Xu, Y. Sheng, et al., "Encapsulation of Printable Mesoscopic Perovskite Solar Cells Enables High Temperature and Long-Term Outdoor Stability," *Advanced Functional Materials* 29, no. 16 (2019): 1809129.

11. A. Uddin, M. B. Upama, H. Yi, and L. Duan, "Encapsulation of Organic and Perovskite Solar Cells: A Review," *Coatings* 9, no. 2 (2019): 65.

12. R. Cheacharoen, K. A. Bush, N. Rolston, D. Harwood, R. H. Dauskardt, and M. G. MD, "Damp Heat, Temperature Cycling and UV Stress Testing of Encapsulated Perovskite Photovoltaic Cells," in *2018 IEEE 7th World Conference on Photovoltaic Energy Conversion, WCPEC 2018—A Joint Conference of 45th IEEE PVSC, 28th PVSEC and 34th EU PVSEC,* vol. 1 (Waikoloha, Hawaii: IEEE, 2018): 3498–3502.

13. M. Bonomo, B. Taheri, L. Bonandini, et al., "Thermosetting Polyurethane Resins as Low-Cost, Easily Scalable, and Effective Oxygen and Moisture Barriers for Perovskite Solar Cells," *ACS Applied Materials & Interfaces* 12, no. 49 (2020): 54862–54875.

14. R. Cheacharoen, C. C. Boyd, G. F. Burkhard, et al., "Encapsulating Perovskite Solar Cells to Withstand Damp Heat and Thermal Cycling," *Sustainable Energy & Fuels* 2, no. 11 (2018): 2398–2406.

15. F. J. Ramos, D. Cortés, A. Aguirre, F. J. Castaño, and S. Ahmad, "Fabrication and Encapsulation of Perovskites Sensitized Solid State Solar Cells," in *2014 IEEE 40th Photovoltaic Specialist Conference (PVSC)* (Denver, Colorado: IEEE, 2014): 2584–2587.

16. L. Luo, P. Liu, K. Zhang, et al., "Vinyl-Functionalized Polyolefins for Fast Photovoltaic Cell Encapsulation," *ACS Applied Polymer Materials* 2 (2020): 2571–2577.

17. Q. Emery, M. Remec, G. Paramasivam, et al., "Encapsulation and Outdoor Testing of Perovskite Solar Cells: Comparing Industrially Relevant Process With a Simplified Lab Procedure," *ACS Applied Materials & Interfaces* 14, no. 4 (2022): 5159–5167.

18. M. Martín, X. Centelles, A. Solé, C. Barreneche, A. I. Fernández, and L. F. Cabeza, "Polymeric Interlayer Materials for Laminated Glass: A Review," *Construction and Building Materials* 230 (2020): 116897.

19. J. Tracy, N. Bosco, C. Delgado, and R. Dauskardt, "Durability of Ionomer Encapsulants in Photovoltaic Modules," *Solar Energy Materials and Solar Cells* 208 (2020): 110397.

20. Y. Wang, I. Ahmad, T. Leung, et al., "Encapsulation and Stability Testing of Perovskite Solar Cells for Real Life Applications," *ACS Materials Au* 2, no. 3 (2022): 215–236.

21. M. D. Kempe, A. A. Dameron, T. J. Moricone, and M. O. Reese, "Evaluation and Modeling of Edge-Seal Materials for Photovoltaic Applications," in *Conference Record of the IEEE Photovoltaic Specialists Conference* (Honolulu, Hawaii: IEEE, 2010): 256–261.

22. L. Shi, T. L. Young, J. Kim, et al., "Accelerated Lifetime Testing of Organic-Inorganic Perovskite Solar Cells Encapsulated by Polyisobutylene," *ACS Applied Materials & Interfaces* 9, no. 30 (2017): 25073–25081.

23. F. Sahli, J. Werner, B. A. Kamino, et al., "Fully Textured Monolithic Perovskite/Silicon Tandem Solar Cells With 25.2% Power Conversion Efficiency," *Nature Materials* 17, no. 9 (2018): 820–826.

24. E. A. Gaulding, A. E. Louks, M. Yang, et al., "Package Development for Reliability Testing of Perovskites," *ACS Energy Letters* 7, no. 8 (2022): 2641–2645.

25. E. Booker, J. B. Boutin, C. Roux, M. Manceau, S. Berson, and S. Cros, "Perovskite Test: A High Throughput Method to Screen Ambient Encapsulation Conditions," *Energy Technology* 8, no. 12 (2020): 2000041.

26. M. Majorel, Thesis manuscript "Développement d'un Adhésif UV-Polymérisable aux Propriétés Optimisées pour l'Encapsulation de Cellules Solaires Pérovskites Flexibles" (2022).

27. S. Ogier, C. Vidal, D. Chapron, et al., "A Comparative Study of Calorimetric Methods to Determine the Crosslinking Degree of the Ethylene-*co*-Vinyl Acetate Polymer Used as a Photovoltaic Encapsulant," *Journal of Polymer Science Part B: Polymer Physics* 55, no. 11 (2017): 866–876.

28. M. Firon, S. Cros, and P. Trouslard, "Method and Device for Measurement of Permeation" (2007, US).

29. A. Morlier, S. Cros, J. P. Garandet, and N. Alberola, "Structural Properties of Ultraviolet Cured Polysilazane Gas Barrier Layers on Polymer Substrates," *Thin Solid Films* 550 (2014): 85–89.

30. D. E. Mansour, S. Mitterhofer, C. Herzog, et al., "Correlation Between EVA Degree of Crosslinking and Moisture Ingress Into PV Laminates," EU PVSEC (2020).

31. C. Barretta, L. Meinhart, H. Krebs, et al.,"Design and Testing of PV Modules Based on Glass/Glass Configuration to Achieve Extended Lifetime," in *40th European Photovoltaic Solar Energy Conference and Exhibition (EU PVSEC 2023)* Lisbon, Portugal: WIP, 2023).

32. S. Baumann, G. E. Eperon, A. Virtuani, et al., "Stability and Reliability of Perovskite Containing Solar Cells and Modules: Degradation Mechanisms and Mitigation Strategies," *Energy & Environmental Science* 17, no. 20 (2024): 7566–7599.

33. G. Griffini and S. Turri, "Polymeric Materials for Long-Term Durability of Photovoltaic Systems," *Journal of Applied Polymer Science* 133, no. 11 (2015): 43080.

34. L. Shi, M. P. Bucknall, T. L. Young, et al., "Gas Chromatography–Mass Spectrometry Analyses of Encapsulated Stable Perovskite Solar Cells," *Science* 368, no. 6497 (2020): eaba2412.

35. M. De Bastiani, G. Armaroli, R. Jalmood, et al., "Mechanical Reliability of Fullerene/Tin Oxide Interfaces in Monolithic Perovskite/Silicon Tandem Cells," *ACS Energy Letters* 7, no. 2 (2022): 827–833.

36. R. Cheacharoen, N. Rolston, D. Harwood, K. A. Bush, R. H. Dauskardt, and M. D. McGehee, "Design and Understanding of Encapsulated Perovskite Solar Cells to Withstand Temperature Cycling," *Energy & Environmental Science* 11, no. 1 (2018): 144–150.

37. A. K. Gupta, *Characterization of Polymers and Fibres, in Manufactured Fibre Technology* (Dordrecht: Springer, 1997).

38. A. Paar, "Basics of Dynamic Mechanical Analysis (DMA)," May 2, 2024, https://wiki.anton-paar.com/ca-fr/basics-of-dynamic-mechanical-analysis-dma/.

39. R. P. Chartoff, J. D. Menczel, and S. H. Dillman, "Dynamic Mechanical Analysis (DMA)," in *Thermal Analysis of Polymers: Fundamentals and Applications*, eds. J. D. Menczel and R. B. Prime (Hoboken, NJ:John Wiley & Sons, Inc., 2008).

Supporting Information

Additional supporting information can be found online in the Supporting Information section.